PERGAMON

International Journal of Solids and Structures 37 (2000) 7105–7126

INTERNATIONAL JOURNAL OF SOLIDS and STRUCTURES

www.elsevier.com/locate/ijsolstr

Cosserat modelling of size effects in the mechanical behaviour of polycrystals and multi-phase materials

Samuel Forest *, Fabrice Barbe, Georges Cailletaud

Ecole des Mines de Paris/CNRS, Centre des Matériaux/UMR 7633, BP 87, 91003 Evry, France

Received 10 November 1999

Abstract

Classical homogenization techniques are not designed to predict the effect of the size of the constituents on the effective mechanical behaviour of heterogeneous materials. They usually take the volume fraction and, in some cases, the morphology of phase distribution into account. This shortcoming is related to the fact that, in crystals, the elastoviscoplastic behaviour of each constituent within the aggregate may be different from that observed on the constituent alone (say the single crystal). Cosserat single crystal plasticity is used in this work to describe the influence of grain size on the effective hardening behaviour of polycrystals. For that purpose, three-dimensional finite element calculations of periodic Cosserat multi-crystalline aggregates of different grain sizes are provided. The polycrystal is regarded as a heterogeneous Cosserat medium and specific techniques for the estimation of the effective properties are presented. The approach is then applied to the case of two-phase single crystal materials for which the behaviour of one phase as a matrix turns out to be much harder than the isolated phase.

Keywords: Cosserat modelling; Mechanical behaviour; Multi-phase materials

1. Introduction

Efficient homogenization techniques are available to derive the overall mechanical properties of heterogeneous materials. They have been successful in describing the global response of non-linear composites with almost periodic micro-structures as well as random materials such as polycrystals (Sanchez-Palencia and Zaoui, 1985). However, several major features of materials micro-structure have been disregarded in the previous analyses. In particular, the effective properties deduced from classical homogenization theories do not depend on the absolute size of heterogenities but only on their volume fraction and, at best, on the morphology of the constituents. In contrast, it is well known in experimental metallurgy that micro-structures can be optimized for the desired overall non-linear properties by varying the size of inclusions or grains. In the present work, we investigate how far the mechanics of generalized continua can help, by including size effects into the framework of the mechanics of heterogeneous materials.

* Corresponding author. Tel.: +33-1-60-76-30-51; fax: +33-1-60-76-31-50.
E-mail address: samuel.forest@mat.ensmp.fr (S. Forest).

0020-7683/00/$ - see front matter
PII: S0020-7683(99)00330-3

Generalized continua can be classified into three main groups. Higher grade media involve higher order gradients of the displacement field or of some internal variables. In the higher order media, independent degrees of freedom are introduced in addition to the usual displacements. Fully non-local media are characterized by an integral formulation of the constitutive equations (Eringen, 1976). In this work, attention is drawn to the Cosserat continuum for which independent displacement $\underline{\mathbf{u}}$ and micro-rotation $\underline{\mathbf{\Phi}}$ degrees of freedom are attributed to each material point. The vector $\underline{\mathbf{\Phi}}$ describes the rotation of an underlying tryad of rigid directors. Deformation and curvature tensors will be defined in Section 2, so that there exist two associated stress tensors: the force-stress tensor $\underset{\sim}{\boldsymbol{\sigma}}$ and the couple-stress tensor $\underset{\sim}{\boldsymbol{\mu}}$. They are not necessarily symmetric. Two balance equations must be fulfilled, namely the balance of momentum and the balance of moment of momentum:

$$\begin{aligned} &\underset{\sim}{\boldsymbol{\sigma}} \cdot \underline{\nabla} = 0, \quad \sigma_{ij,j} = 0, \\ &\underset{\sim}{\boldsymbol{\mu}} \cdot \underline{\nabla} - \underset{\simeq}{\boldsymbol{\epsilon}} : \underset{\sim}{\boldsymbol{\sigma}} = 0, \quad \mu_{ij,j} - \epsilon_{ijk}\sigma_{jk} = 0, \end{aligned} \tag{1}$$

where volume forces and couples have been excluded for simplicity. A complete account of the Cosserat theory can be found in Eringen (1976) and a special case, the so-called couple-stress theory, has been extensively studied by Koiter (1963). The links between the Cosserat continuum and crystal plasticity are presented in Section 2. The key argument is the introduction of the so-called dislocation density tensor (Nye, 1953) into the traditional constitutive framework for single crystals as settled by Mandel (1965, 1971). In other terms, this corresponds to a distinction in the set of internal variables between the densities of the so-called statistically stored and geometrically necessary dislocations (Fleck and Hutchinson, 1997). An extension of the classical multiplicative large deformation single crystal theory to the Cosserat framework is recalled in Section 2.2, to insist on the natural definition of an intermediate released configuration for both force and couple stresses. The remainder of this work deals with the small perturbation framework. Some applications of Cosserat crystal plasticity to localization phenomena have been reported in Forest (1998). The aim of the present work is to show the ability of generalized single crystal plasticity to account for some size effects in crystals.

The available computational tools are now sufficient to carry out finite element calculations on a volume element of polycrystal containing enough grains to regard it as representative (Eberl et al., 1998). The main advantage of this approach, in comparison with standard bounding or estimation techniques of homogenization, lies in the fact that it provides not only the effective response of the polycrystal but also an insight into the heterogeneous intragranular stress-deformation state. The polycrystalline aggregates presented in this work are simulated as Voronoï polyhedra and the corresponding finite element meshes are such that each grain contains enough integration points to give a quite accurate description of the deformation patterns within the grains. In this work, each grain is treated as a Cosserat single crystal so that the polycrystal must be dealt with as a heterogeneous Cosserat aggregate. That is why the basic tools of homogenization theory must be extended to heterogeneous Cosserat materials. Some of them, including average relations between local and global mechanical quantities, are presented in Section 3, namely an extension of the Hill–Mandel approach and the case of periodic micro-structures. An extension of variational methods to derive bounds for the effective properties to generalized continua can be found in Smyshlyaev and Fleck (1996), where a first approach of grain size effects using strain gradient non-linear elasticity has been proposed.

It is well known that the apparent yield strength σ_0 in tension of polycrystalline metals tends to increase with decreasing grain size (Jaoul, 1965). The famous Hall–Petch relationship:

$$\sigma_0 = \sigma_\mathrm{m} + kD^{-1/2}, \tag{2}$$

where D is the grain size, k a constant and σ_m an asymptotic yield stress for the single crystal, has been checked in the case of b.c.c. crystals. For the f.c.c. crystals considered in this work, the polycrystal tends to

behave like the most resistant single crystal orientation but the hardening capability of the polycrystal still increases with decreasing grain size. Weng (1983) suggested to write relation (2) at the level of resolved shear stresses of slip systems. He proposed a self-consistent scheme for polycrystalline elastoplasticity including grain size effects. The influence of the grain size on the hardening of the material was also introduced in a somewhat more complicated expression than (2). Such a formulation seems to be legitimate in the case of mean-field models such as the self-consistent one, for which the mean stress and strain over all grains having the same orientation only is considered. If, in addition to this, one is interested in the intragranular stress–strain distributions within a polycrystalline aggregate, relation (2) is not applicable any more in each material point of each grain. The evolution of the critical resolved shear stresses will be different in the core of the grain, in the neighbourhood of grain boundaries or free surfaces. It is claimed in this work that some of these features can be captured using generalized crystal plasticity. For this purpose, we will consider in Section 4 an initial boundary value problem for an aggregate of Cosserat crystals with a varying grain size. A rather small number of grains will be considered due to the large number of degrees of freedom and internal variables associated with the Cosserat model. Periodicity has been retained for these simulations.

The proposed approach can in principle be applied to describe more general size effects than the previously mentioned grain size effects, and in particular to model composite material reinforcement by inclusions or precipitates of different sizes in a metal matrix. The problem of precipitate hardening is addressed in the last section of this work, with a specific example of two-phase nickel-based superalloys. The use of generalized crystal plasticity in this case is relevant if hardening effects are due to the formation of dislocation pile-ups at precipitates or, using another terminology, when the storage of geometrically necessary dislocations near precipitates leads to additional hardening of the material. The fact that the in situ behaviour of a constituent may be strongly different from that of the bulk material is a major feature of the mechanics of non-linear heterogeneous materials. The mechanics of generalized continua can help to take this aspect into account. This is also the occasion of setting the limits of the approach, at the borderline between discrete dislocation simulation and continuum mechanics.

In this work, $\underline{\mathbf{a}}$, $\underset{\sim}{\mathbf{a}}$, $\underset{\approx}{\boldsymbol{a}}$ and $\underset{\approx}{\mathbf{a}}$ denote respectively a vector, a second-rank, a third-rank and a fourth-rank tensor. The nabla operator reads $\underline{\mathbf{V}}$. The gradient of the displacement field is $\underset{\sim}{\mathbf{f}} = \underline{\mathbf{u}} \otimes \underline{\mathbf{V}} = u_{i,j}\underline{\mathbf{e}}_i \otimes \underline{\mathbf{e}}_j$, where $\{\underline{\mathbf{e}}_i\}_{i=1,2,3}$ is an orthonormal basis and $\otimes$ the dyadic product. The symmetric and skew-symmetric parts of $\underset{\sim}{\mathbf{f}}$ are respectively denoted $^{\{}\underset{\sim}{\mathbf{f}}^{\}} = \underset{\sim}{\boldsymbol{\varepsilon}}$ and $^{\}}\underset{\sim}{\mathbf{f}}^{\{}$. The indices notation is used when the intrinsic one may become ambiguous.

2. Cosserat single crystal plasticity

2.1. Overall description of dislocation populations

The yielding and hardening behaviour of crystals mainly depends on the growth of the dislocation population and on the development of dislocation structures inside the volume element V of continuum mechanics. A precise account of the evolution of dislocation distribution in V still lies beyond current computing capacity, although promising results in that field are available (Fivel and Canova, 1998). The incomplete information about the dislocation state permits probability predictions and suggests the use of statistical mechanics. Kröner (1969) proposed that the information be given in terms of n-point dislocation correlation tensor functions. If the vectors $\underline{\boldsymbol{\xi}}(\underline{\mathbf{x}})$ and $\underline{\mathbf{b}}(\underline{\mathbf{x}})$ describe the line vector and Burgers vector of a dislocation located at $\underline{\mathbf{x}}$, the first correlation function reads:

$$\underset{\sim}{\boldsymbol{\alpha}} = \langle \underline{\mathbf{b}} \otimes \underline{\boldsymbol{\xi}} \rangle, \tag{3}$$

where the brackets denote ensemble averaging. Then, the next correlation function is:

$$\underset{\approx}{\boldsymbol{\alpha}}(\underline{\mathbf{x}}, \underline{\mathbf{x}}') = \langle (\underline{\mathbf{b}} \otimes \underline{\boldsymbol{\xi}})(\underline{\mathbf{x}}) \otimes (\underline{\mathbf{b}} \otimes \underline{\boldsymbol{\xi}})(\underline{\mathbf{x}}') \rangle = \underset{\approx}{\boldsymbol{\alpha}}(\underline{\mathbf{x}} - \underline{\mathbf{x}}') \tag{4}$$

if statistical uniformity is assumed. Second- and fourth-rank tensors $\underset{\sim}{\boldsymbol{\alpha}}$ and $\underset{\approx}{\boldsymbol{\alpha}}$ are indeed related to classical plastic state indicators used in classical crystal plasticity. For a large enough volume element V, it is resorted to the ergodic hypothesis so that ensemble averaging is replaced by volume averaging over V. In this case, $\underset{\sim}{\boldsymbol{\alpha}}$ turns out to be identical to the so-called dislocation density tensor, or Nye's tensor, which is the basic variable of the continuum theory of dislocations (Nye, 1953). On the contrary, one invariant of the tensor $\underset{\approx}{\boldsymbol{\alpha}}$ can be shown to be

$$\boldsymbol{\alpha}_{ijij}(\underline{\mathbf{0}}) = L/V = \rho, \tag{5}$$

where L is the length of dislocation lines inside V. The dislocation density ρ is well known in the field of metallurgy.

Modern crystal plasticity (Mandel, 1971) relies on the use of internal variables that are more or less related to ρ rather than $\underset{\sim}{\boldsymbol{\alpha}}$, and has proved to be efficient in describing the main features of the deformation behaviour of single crystals under tensile, shear and, to some extent, non-homogeneous loading conditions. Quantities $\underset{\sim}{\boldsymbol{\alpha}}$ and ρ are independent moments of the same distribution and, in principle, should both enter the constitutive framework (Forest et al., 1997). The dislocation density tensor can be related to the plastic incompatibility by

$$\underset{\sim}{\boldsymbol{\alpha}} = -\underset{\sim}{\mathrm{curl}}\ \underset{\sim}{\mathbf{f}}^{\mathrm{p}} = -\epsilon_{jkl} f^{\mathrm{p}}_{ik,l}\, \underline{\mathbf{e}}_i \otimes \underline{\mathbf{e}}_j, \tag{6}$$

where $\underset{\sim}{\mathbf{f}} = \underset{\sim}{\mathbf{f}}^{\mathrm{e}} + \underset{\sim}{\mathbf{f}}^{\mathrm{p}}$ has been decomposed into elastic and plastic parts (Kröner, 1958). It means that, if $\underset{\sim}{\boldsymbol{\alpha}}$ is introduced as an additional internal variable in the constitutive theory of crystals, it will have a non-local character as is related to the gradient of the plastic deformation. Such a theory has been used in Dai and Parks (1997). In this case, the mechanical framework remains classical and the thermodynamical force associated with $\underset{\sim}{\boldsymbol{\alpha}}$ does not enter the mechanical balance equations. A perhaps more ambitious approach, presented in Shu et al. (1996) and Fleck and Hutchinson (1997), consists in acknowledging the fact that, once a variable such as $\underset{\sim}{\boldsymbol{\alpha}}$ is introduced, the material cannot be regarded as simple any more. For completeness, $\underset{\sim}{\boldsymbol{\varepsilon}} \otimes \underline{\nabla}$ or equivalently the second gradient of the displacement field should be introduced, which leads to a full second grade medium (Germain, 1973). The authors Shu et al. (1996) and Fleck and Hutchinson (1997) then propose a full constitutive framework for elastoplastic second grade single crystals. In particular, a generalized criterion and flow rules are postulated.

On the contrary, Eq. (6) can be rewritten in terms of the gradient of lattice rotation:

$$\underset{\sim}{\boldsymbol{\alpha}} = \underset{\sim}{\boldsymbol{\kappa}}^{\mathrm{T}} - (\mathrm{tr}\ \underset{\sim}{\boldsymbol{\kappa}})\underset{\sim}{\mathbf{1}} + \underset{\sim}{\mathrm{curl}}\ \underset{\sim}{\boldsymbol{\varepsilon}}^{\mathrm{e}}, \tag{7}$$

where $\underset{\sim}{\boldsymbol{\varepsilon}}^{\mathrm{e}} = \{\ \underset{\sim}{\mathbf{f}}^{\mathrm{e}}\}$. Setting its skew-symmetric part $\}\underset{\sim}{\mathbf{f}}^{\mathrm{e}}\{ = -\underset{\approx}{\epsilon} \cdot \underline{\boldsymbol{\Phi}}$, the lattice torsion curvature is defined by

$$\underset{\sim}{\boldsymbol{\kappa}} = \underline{\boldsymbol{\Phi}} \otimes \underline{\nabla} = \boldsymbol{\Phi}_{i,j}\underline{\mathbf{e}}_i \otimes \underline{\mathbf{e}}_j. \tag{8}$$

The manifestation of $\underset{\sim}{\boldsymbol{\alpha}}$ turns out to be the existence of lattice curvature which can be decomposed into elastic and plastic parts $\underset{\sim}{\boldsymbol{\kappa}}^{\mathrm{e}}$ and $\underset{\sim}{\boldsymbol{\kappa}}^{\mathrm{p}}$. The thermodynamic force associated with $\underset{\sim}{\boldsymbol{\kappa}}^{\mathrm{e}}$ is a couple-stress tensor that can influence the equilibrium state of the solid and should therefore enter the equation of balance of moment of momentum of the medium. This can be done within the framework of the Cosserat theory. The motivations and developments of the theory can be found in Forest et al. (1997). Again, a full constitutive framework including evolution rules for plastic curvature has been postulated and is briefly recalled in Section 2.2.

2.2. General framework

Cosserat single crystal elastoviscoplasticity represents a generalization of the anisotropic plasticity framework settled by Mandel (1973). In particular, it can be formulated for arbitrary deformation, micro-

rotation and torsion-curvature. The independent degrees of freedom are the displacement $\underline{\mathbf{u}}(\underline{\mathbf{x}},t)$ and lattice rotation $\underset{\sim}{\mathbf{R}}(\underline{\mathbf{x}},t)$, meaning that a tryad of rigid vectors is attached to each material point. The vectors are supposed to coincide at each time with the same lattice vectors in the released configuration at point $\underline{\mathbf{x}}$. The different configurations are defined in Fig. 1 (Sievert et al., 1998).

The deformation gradient $\underset{\sim}{\mathbf{F}}$ and the lattice torsion-curvature tensor $\underset{\sim}{\mathbf{\Gamma}}$ are defined by

$$\underset{\sim}{\mathbf{F}} = \underset{\sim}{\mathbf{1}} + \underline{\mathbf{u}} \otimes \underline{\nabla} = (\delta_{ij} + u_{i,j})\underline{\mathbf{e}}_i \otimes \underline{\mathbf{e}}_j \quad \text{and} \quad \underset{\sim}{\mathbf{\Gamma}} = \tfrac{1}{2}\underset{\approx}{\epsilon} : (\underset{\sim}{\mathbf{R}}(\underset{\sim}{\mathbf{R}}^{\mathrm{T}} \otimes \underline{\nabla})) = \tfrac{1}{2}\epsilon_{ikl}R_{km}R_{lm,j}\underline{\mathbf{e}}_i \otimes \underline{\mathbf{e}}_j. \tag{9}$$

Note that the previously defined tensor $\underset{\sim}{\boldsymbol{\kappa}}$ corresponds to the small perturbation approximation of $\underset{\sim}{\mathbf{\Gamma}}$. When written in the space frame associated with $\underset{\sim}{\mathbf{R}}(\underline{\mathbf{x}})$ at point $\underline{\mathbf{x}}$, it reads:

$$^{\sharp}\underset{\sim}{\mathbf{F}} = \underset{\sim}{\mathbf{R}}^{\mathrm{T}}\underset{\sim}{\mathbf{F}}, \qquad ^{\sharp}\underset{\sim}{\mathbf{\Gamma}} = \underset{\sim}{\mathbf{R}}^{\mathrm{T}}\underset{\sim}{\mathbf{\Gamma}}. \tag{10}$$

Deformation and curvature can be decomposed into their elastic and plastic parts as follows:

$$^{\sharp}\underset{\sim}{\mathbf{F}} = {}^{\sharp}\underset{\sim}{\mathbf{F}}^{\mathrm{e}}{}^{\sharp}\underset{\sim}{\mathbf{F}}^{\mathrm{p}} \quad \text{and} \quad ^{\sharp}\underset{\sim}{\mathbf{\Gamma}} = {}^{\sharp}\underset{\sim}{\mathbf{\Gamma}}^{\mathrm{e}}{}^{\sharp}\underset{\sim}{\mathbf{F}}^{\mathrm{p}} + {}^{\sharp}\underset{\sim}{\mathbf{\Gamma}}^{\mathrm{p}}. \tag{11}$$

These two decompositions enable us to define an intermediate configuration for which both force and couple stresses are released (Sievert et al., 1998).

In the case of small micro-rotations and small curvatures, the lattice rotation vector $\underline{\mathbf{\Phi}}$ and the torsion-curvature tensor are defined by:

$$\underset{\sim}{\mathbf{R}} = \underset{\sim}{\mathbf{1}} - \underset{\approx}{\epsilon} \cdot \underline{\mathbf{\Phi}} \quad \text{and} \quad \underset{\sim}{\boldsymbol{\kappa}} = \underline{\mathbf{\Phi}} \otimes \underline{\nabla} = \underset{\sim}{\boldsymbol{\kappa}}^{\mathrm{e}} + \underset{\sim}{\boldsymbol{\kappa}}^{\mathrm{p}}. \tag{12}$$

Similarly, within the small perturbation framework, an adequate Cosserat deformation measure reads

$$\underset{\sim}{\mathbf{e}} = \underline{\mathbf{u}} \otimes \underline{\nabla} + \underset{\approx}{\epsilon} \cdot \underline{\mathbf{\Phi}} = \underset{\sim}{\mathbf{e}}^{\mathrm{e}} + \underset{\sim}{\mathbf{e}}^{\mathrm{p}} \tag{13}$$

The elasticity law in the isotropic case is given as

$$\underset{\sim}{\boldsymbol{\sigma}} = \underset{\approx}{\mathbf{E}} : \underset{\sim}{\mathbf{e}}^{\mathrm{e}} = \lambda \underset{\sim}{\mathbf{1}}\,\mathrm{Tr}\,\underset{\sim}{\mathbf{e}}^{\mathrm{e}} + 2\mu^{\{}\underset{\sim}{\mathbf{e}}^{\mathrm{e}\}} + 2\mu_{\mathrm{c}}{}^{\}}\underset{\sim}{\mathbf{e}}^{\mathrm{e}\{}, \tag{14}$$

$$\underset{\sim}{\boldsymbol{\mu}} = \underset{\approx}{\mathbf{C}} : \underset{\sim}{\boldsymbol{\kappa}}^{\mathrm{e}} = \alpha \underset{\sim}{\mathbf{1}}\,\mathrm{Tr}\,\underset{\sim}{\boldsymbol{\kappa}}^{\mathrm{e}} + 2\beta^{\{}\underset{\sim}{\boldsymbol{\kappa}}^{\mathrm{e}\}} 2\gamma^{\}}\underset{\sim}{\boldsymbol{\kappa}}^{\mathrm{e}\{}, \tag{15}$$

which involves six elasticity moduli, the two classical ones and four additional ones. Plastic deformation is due to the activation of slip systems according to

$$\dot{\underset{\sim}{\mathbf{e}}}^{\mathrm{p}} = \sum_{s=1}^{n} \dot{\gamma}^s \underset{\sim}{\mathbf{P}}^s, \tag{16}$$

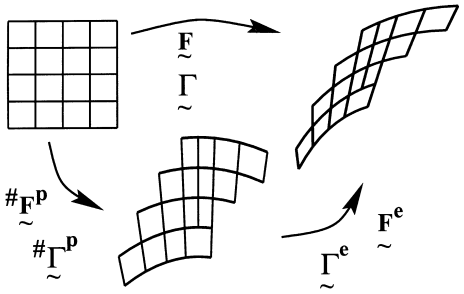

Fig. 1. Kinematics of Cosserat single crystal plasticity.

where the so-called orientation tensor $\underset{\sim}{\mathbf{P}}^s$ is defined by

$$\underset{\sim}{\mathbf{P}}^s = \underline{\mathbf{m}}^s \otimes \underline{\mathbf{n}}^s. \tag{17}$$

This corresponds to multi-mechanisms plasticity for which a general framework has been settled by Koiter (1960) and Mandel (1965). Vector $\underline{\mathbf{m}}^s$ and $\underline{\mathbf{n}}^s$, respectively, are the slip direction and the normal to the slip plane for slip system s. Similarly, plastic torsion-curvature orientation tensors $\underset{\sim}{\mathbf{Q}}_\perp$ and $\underset{\sim}{\mathbf{Q}}_\odot$ exist such that

$$\underset{\sim}{\boldsymbol{\kappa}}^{\mathrm{p}} = \sum_{s=1}^{n} \left(\frac{\dot{\theta}^s_\perp}{l_\perp} \underset{\sim}{\mathbf{Q}}^s_\perp + \frac{\dot{\theta}^s_\odot}{l_\odot} \underset{\sim}{\mathbf{Q}}^s_\odot \right), \tag{18}$$

where $l_\perp$, $l_\odot$ are constitutive characteristic lengths. The index $\perp$ denotes the lattice curvature due to edge dislocations and $\odot$ indicates the lattice torsion due to screw dislocations. The continuum theory of dislocations provides a relation between the dislocation density tensor and the torsion-curvature tensor as in Eq. (7) (Forest et al., 1997), from which we deduce

$$\underset{\sim}{\mathbf{Q}}^s_\perp = \underline{\boldsymbol{\xi}}^s \otimes \underline{\mathbf{m}}^s, \qquad \underset{\sim}{\mathbf{Q}}^s_\odot = \tfrac{1}{2}\underset{\sim}{\mathbf{1}} - \underline{\mathbf{m}}^s \otimes \underline{\mathbf{m}}^s, \tag{19}$$

where $\underline{\boldsymbol{\xi}}^s = \underline{\mathbf{n}}^s \times \underline{\mathbf{m}}^s$ is the edge dislocation line vector. In this work, the additional internal variables $\theta^s_\perp$ only are taken into account and the length $l_\perp$ will be called l_{p} in the sequel.

2.3. Identification of material parameters

Eqs. (16)–(18) describe the kinematics of elastoplastic Cosserat crystals. The set of equations must be closed by the flow rules and hardening laws. To avoid any indeterminancy in slip activation, a formulation in viscoplasticity is adopted:

$$\dot{\gamma}^s = \left\langle \frac{|\tau^s| - r^s}{k} \right\rangle^n \operatorname{sign}(\tau^s) \quad \text{and} \quad \dot{\theta}^s = \left\langle \frac{|v^s| - l_{\mathrm{p}} r^s_{\mathrm{c}}}{l_{\mathrm{p}} k^s_{\mathrm{c}}} \right\rangle^{n^s_{\mathrm{c}}} \operatorname{sign}(v^s), \tag{20}$$

where $\tau^s = \underset{\sim}{\mathbf{P}}^s : \underset{\sim}{\boldsymbol{\sigma}}^s$ and $v^s = \underset{\sim}{\mathbf{Q}}^s : \underset{\sim}{\boldsymbol{\mu}}^s$, respectively, are the resolved force and couple stresses on the slip and curvature system s. The quantities in brackets must be positive for the slip and plastic curvature rate to be non-zero. Eq. (20) corresponds to a generalized Schmid law. Parameter k (resp. n) can be chosen low (resp. large) enough for plastic flow to be almost rate independent.

The evolution rules for the thresholds r^s and r^s_{c} used in this work are the following:

$$r^s = r_0 + q \sum_{r=1}^{n} h^{sr} (1 - \exp(-b v^r)) + H' |\theta^s| \quad \text{with } \dot{v}^s = |\dot{\gamma}^s|, \tag{21}$$

$$r^s_{\mathrm{c}} = r_{\mathrm{c}0}.$$

The interaction matrix h^{rs} accounts for self- and latent hardening. The threshold for the plastic curvature is taken to be constant for simplicity. A simple linear coupling term H' is added to more conventional non-linear contributions.

The classical parameters r_0, h^{rs}, q and b can be derived from homogeneous monotonous tests. The additional parameters are α, β, γ, μ_{c} for elasticity and $r_{\mathrm{c}0}, H'$ and l_{p} for plastic curvature. Kröner (1963) derived the flexural rigidity of a crystal element containing a regular lattice of edge dislocations. The bending modulus is found to be proportional to μd^2, where d is half the edge dislocation spacing. We will use very small values of α and $\beta = \gamma$ (as in De Borst, 1991) that correspond to a large enough amount of the so-called geometrically necessary dislocations inside V. We will then assume that the elastic response of the crystal does not significantly deviate from the classical one and, in particular, that elastic rotations are

material rotations. It means that $\underset{\sim}{\mathbf{e}}^{\mathrm{e}}$ is not far from being symmetric. This can be achieved using a large μ_{c} parameter. This corresponds to the constrained Cosserat elasticity or to Koiter's couple-stress theory (Koiter, 1963) as long as the material behaviour remains elastic. Once yielding has begun, lattice rotations deviate from material rotations represented by the skew-symmetric part of $\underset{\sim}{\mathbf{f}}$. As a result, the proposed theory departs from the fully constrained Cosserat theory or couple-stress theory, for which the micro-rotation vector $\underline{\boldsymbol{\Phi}}$ is nothing but the rotation vector associated with skew-symmetric part of the deformation gradient. A low threshold for plastic curvature has been chosen so that the remaining coefficients to be determined are H' and l_{p}. Note that in fact the combination $H'l_{\mathrm{p}}$ (unit MPa m) only is relevant and that the choice of the characteristic length l_{p} becomes conventional. The coupling parameter H' plays a role, when lattice rotation gradients develop and can be identified only under such circumstances. Strain localization phenomena represent situations for which such coupling becomes essential. Slip, shear and kink banding has been studied using this Cosserat model in Forest (1998), and it has been suggested that the measurement of the width of kink bands in single crystals enables one to determine $H'l_{\mathrm{p}}$. In this work, alternative situations are presented that permit its determination, namely, those associated with size effects in crystals. In particular, it will appear in the sequel that the influence of grain size on the overall mechanical response of polycrystals can be described using the coupled hardening law (21). Non-linear coupling terms should also be considered.

3. Overall behaviour of heterogeneous Cosserat materials

The polycrystal can now be regarded as a heterogeneous Cosserat material as it is an aggregate of Cosserat single crystal grains. As a result, some homogenization procedures must be designed to study the resulting properties of the polycrystal. Some estimation methods have been proposed in Dendievel et al. (1998) and applied in the case of the heterogeneous linear Cosserat elasticity.

3.1. Homogenization methods for Cosserat materials

3.1.1. Hill–Mandel approach

The aim is to replace a heterogeneous material by a homogeneous substitute medium (HSM), which can be said to be equivalent in the sense to be made precise. Following Hill–Mandel's approach of the mechanics of heterogeneous materials (Sanchez-Palencia and Zaoui, 1985), a condition of macro-homogeneity is required stipulating that the (isothermal for simplicity) free energy of the HSM at point $\underline{\mathbf{x}}$ can be identified to the mean value of the free energy over a representative volume element V under the same overall loading conditions at $\underline{\mathbf{x}}$. In the case of heterogeneous Cosserat materials for which the local fields are $\underset{\sim}{\mathbf{e}}$, $\underset{\sim}{\boldsymbol{\kappa}}$, $\underset{\sim}{\boldsymbol{\sigma}}$ and $\underset{\sim}{\boldsymbol{\mu}}$ inside V, this condition can be generalized in the following forms: If the overall substitute medium (to be used for structural calculations for instance) is treated as Cauchy continuum, the condition reads:

$$\langle \underset{\sim}{\boldsymbol{\sigma}} : \underset{\sim}{\mathbf{e}} + \underset{\sim}{\boldsymbol{\mu}} : \underset{\sim}{\boldsymbol{\kappa}} \rangle = \underset{\sim}{\boldsymbol{\Sigma}} : \underset{\sim}{\mathbf{E}}, \tag{22}$$

where $\underset{\sim}{\mathbf{E}}$ and $\underset{\sim}{\boldsymbol{\Sigma}}$ are the effective (symmetric) deformation and stress tensors. If the HSM is regarded as a Cosserat continuum itself, it becomes

$$\langle \underset{\sim}{\boldsymbol{\sigma}} : \underset{\sim}{\mathbf{e}} + \underset{\sim}{\boldsymbol{\mu}} : \underset{\sim}{\boldsymbol{\kappa}} \rangle = \underset{\sim}{\boldsymbol{\Sigma}} : \underset{\sim}{\mathbf{E}} + \underset{\sim}{\mathbf{M}} : \underset{\sim}{\mathbf{K}}, \tag{23}$$

where $\underset{\sim}{\mathbf{K}}$ and $\underset{\sim}{\mathbf{M}}$ are effective curvature and couple-stress tensors, $\underset{\sim}{\mathbf{E}}$ and $\underset{\sim}{\boldsymbol{\Sigma}}$ being not necessarily symmetric any more. Procedure (23) is of course more general and contains Eq. (22) as a special case to which it reduces if the effective characteristic length is very small.

The determination of the effective properties then goes through the resolution of a boundary value problem on V. Boundary conditions on ∂V must then be chosen that automatically fulfill conditions (22) or (23). In Dendievel et al. (1998), we have proposed a simple generalization of classical homogeneous conditions at the boundary:

$$\underline{\mathbf{u}} = \underset{\sim}{\mathbf{E}} \cdot \underline{\mathbf{x}} \quad \text{and} \quad \underline{\mathbf{\Phi}} = \underset{\sim}{\mathbf{K}} \cdot \underline{\mathbf{x}} \quad \forall \underline{\mathbf{x}} \in \partial V, \tag{24}$$

where $\underset{\sim}{\mathbf{E}}$ and $\underset{\sim}{\mathbf{K}}$ are given and constant. It follows that

$$\underset{\sim}{\mathbf{E}} = \langle \underline{\mathbf{u}} \otimes \underline{\nabla} \rangle \quad \text{and} \quad \underset{\sim}{\mathbf{K}} = \langle \underset{\sim}{\boldsymbol{\kappa}} \rangle. \tag{25}$$

Condition (23) is then automatically satisfied for the following definition of the effective stress tensors:

$$\underset{\sim}{\mathbf{\Sigma}} = \langle \underset{\sim}{\boldsymbol{\sigma}} \rangle \quad \text{and} \quad \underset{\sim}{\mathbf{M}} = \langle \underset{\sim}{\boldsymbol{\mu}} + (\underset{\approx}{\boldsymbol{\epsilon}} : \underset{\sim}{\boldsymbol{\sigma}}) \otimes \underline{\mathbf{x}} \rangle = \langle \mu_{ij} + \epsilon_{imn} \sigma_{mn} x_j \rangle \underline{\mathbf{e}}_i \otimes \underline{\mathbf{e}}_j. \tag{26}$$

This homogenization procedure has also been proposed in De Felice and Rizzi (1997).

3.1.2. Asymptotic methods

In the case of periodic micro-structures, a unit cell V can be defined and asymptotic methods are well adapted for deriving the form of the effective balance and constitutive equations (Sanchez-Palencia, 1974). The key point is the choice of the small parameter ε introduced in the multi-scale asymptoic developments. Two different schemes have been proposed in Forest and Sab (1998) for periodic heterogeneous Cosserat media. Three characteristic lengths must be distinguished: the size l of the unit cell V, a typical characteristic length l_c of the constituents of the heterogeneous Cosserat material, and a typical wavelength L_ω associated with the applied loading conditions. In the classical homogenization theory, one usually speaks of slowly varying the mean fields when $l \ll L_\omega$ and, in this case, the small parameter is $\varepsilon = l/L_\omega$. In the present situation, one may first consider a limiting process $\mathscr{H}^{\mathrm{I}}$ with $\varepsilon \to 0$, for which the Cosserat length scale varies in the same way as l, so that the small parameter can also be written $\varepsilon = l_c/L_\omega$. In this case, the effective medium can be shown to be a Cauchy continuum (Forest and Sab, 1998). According to a second limiting process $\mathscr{H}^{\mathrm{II}}$, l_c is kept constant, which corresponds to $\varepsilon = l/l_c$. The main fields are now treated as functions of the two variables $\underline{\mathbf{x}}$ and $\underline{\mathbf{y}} = \underline{\mathbf{x}}/\varepsilon$. The local fields can be expanded in power series of ε,

$$\underline{\mathbf{u}}^\varepsilon(\underline{\mathbf{x}}) = \underline{\mathbf{u}}^0(\underline{\mathbf{x}}, \underline{\mathbf{y}}) + \varepsilon \underline{\mathbf{u}}^1(\underline{\mathbf{x}}, \underline{\mathbf{y}}) + \varepsilon^2 \underline{\mathbf{u}}^2(\underline{\mathbf{x}}, \underline{\mathbf{y}}) + \cdots, \tag{27}$$

$$\underline{\mathbf{\Phi}}^\varepsilon(\underline{\mathbf{x}}) = \underline{\mathbf{\Phi}}^0(\underline{\mathbf{x}}, \underline{\mathbf{y}}) + \varepsilon \underline{\mathbf{\Phi}}^1(\underline{\mathbf{x}}, \underline{\mathbf{y}}) + \varepsilon^2 \underline{\mathbf{\Phi}}^2(\underline{\mathbf{x}}, \underline{\mathbf{y}}) + \cdots, \tag{28}$$

where the $\underline{\mathbf{u}}^i$ and $\underline{\mathbf{\Phi}}^i$ are assumed to have the same order of magnitude and are periodic in $\underline{\mathbf{y}}$. Similar expansions exist for the force and couple stresses:

$$\underset{\sim}{\boldsymbol{\sigma}}^\varepsilon(\underline{\mathbf{x}}) = \underset{\sim}{\boldsymbol{\sigma}}^0(\underline{\mathbf{x}}, y) + \varepsilon \sigma^1(\underline{\mathbf{x}}, \underline{\mathbf{y}}) + \varepsilon^2 \underset{\sim}{\boldsymbol{\sigma}}^2(\underline{\mathbf{x}}, \underline{\mathbf{y}}) + \cdots, \tag{29}$$

$$\underset{\sim}{\boldsymbol{\mu}}^\varepsilon(\underline{\mathbf{x}}) = \underset{\sim}{\boldsymbol{\mu}}^0(\underline{\mathbf{x}}, y) + \varepsilon \mu^1(\mathbf{x}, \underline{\mathbf{y}}) + \varepsilon^2 \boldsymbol{\mu}^2(\underline{\mathbf{x}}, \underline{\mathbf{y}}) + \cdots. \tag{30}$$

The form of the constitutive equations is different for each homogenization procedure and in the case of linear elasticity (Forest and Sab, 1998), they read:

$$\mathscr{H}^{\mathrm{I}} : \underset{\sim}{\boldsymbol{\sigma}}^\varepsilon = \underset{\approx}{\mathbf{D}}(\underline{\mathbf{y}}) : \underset{\sim}{\mathbf{e}}^\varepsilon(\underline{\mathbf{x}}) \quad \text{and} \quad \underset{\sim}{\boldsymbol{\mu}}^\varepsilon = \varepsilon^2 \underset{\approx}{\mathbf{C}}(\underline{\mathbf{y}}) : \underset{\sim}{\boldsymbol{\kappa}}^\varepsilon(\underline{\mathbf{x}}), \tag{31}$$

$$\mathscr{H}^{\mathrm{II}} : \underset{\sim}{\boldsymbol{\sigma}}^\varepsilon = \underset{\approx}{\mathbf{D}}(\underline{\mathbf{y}}) : \underset{\sim}{\mathbf{e}}^\varepsilon(\underline{\mathbf{x}}) \quad \text{and} \quad \underset{\sim}{\boldsymbol{\mu}}^\varepsilon = \underset{\approx}{\mathbf{C}}(\underline{\mathbf{y}}) : \underset{\sim}{\boldsymbol{\kappa}}^\varepsilon(\underline{\mathbf{x}}). \tag{32}$$

After noting that $\underline{\nabla} = \underline{\nabla}_x + 1/\varepsilon \underline{\nabla}_y$ (with obvious notations), we compute the gradient of the kinematic variables and the divergence of the stresses in order to introduce them in the balance equations (1) and in the constitutive equations. Ordering the terms according to ε leads to a set of equations from which a series of auxiliary boundary value problems to be solved on the unit cell can be defined (see Boutin (1996) for a classical case). The first auxiliary problem for the procedure $\mathscr{H}^{\mathrm{II}}$ consists in determining vector fields $\underline{\mathbf{v}}$ and $\underline{\boldsymbol{\psi}}$ such that:

$$\underline{\mathbf{u}} = \underset{\sim}{\mathbf{E}} \cdot \underline{\mathbf{y}} + \underline{\mathbf{v}} \quad \text{and} \quad \underline{\boldsymbol{\Phi}} = \underset{\sim}{\mathbf{K}} \cdot \underline{\mathbf{y}} + \underline{\boldsymbol{\psi}} \quad \forall \underline{\mathbf{y}} \in V, \tag{33}$$

$$\underset{\sim}{\boldsymbol{\sigma}} = \underset{\approx}{\mathbf{D}} : (\underline{\mathbf{u}} \otimes \underline{\nabla}_y) \quad \text{and} \quad \underset{\sim}{\boldsymbol{\mu}} = \underset{\approx}{\mathbf{C}} : (\underline{\boldsymbol{\Phi}} \otimes \underline{\nabla}_y), \tag{34}$$

$$\underset{\sim}{\boldsymbol{\sigma}} \cdot \underline{\nabla}_y = 0 \quad \text{and} \quad \underset{\sim}{\boldsymbol{\mu}} \cdot \underline{\nabla}_y = 0, \tag{35}$$

where $\underline{\mathbf{v}}$ and $\underline{\boldsymbol{\psi}}$ take the same values on opposite sides of the cell and the traction and surface couple vectors $\underset{\sim}{\boldsymbol{\sigma}} \cdot \underline{\mathbf{n}}$ and $\underset{\sim}{\boldsymbol{\mu}} \cdot \underline{\mathbf{n}}$ are anti-periodic. The solution of this problem gives in fact the terms $\underline{\mathbf{u}}_1, \underline{\boldsymbol{\Phi}}_1, \underset{\sim}{\boldsymbol{\sigma}}^0$ and $\underset{\sim}{\boldsymbol{\mu}}^0$ of the expansion. This leads to the following expression of the mean work of internal forces:

$$\langle \underset{\sim}{\boldsymbol{\sigma}} : \underset{\sim}{\mathbf{e}} + \underset{\sim}{\boldsymbol{\mu}} : \underset{\sim}{\boldsymbol{\kappa}} \rangle = \langle \underset{\sim}{\boldsymbol{\sigma}} \rangle : \langle \underline{\mathbf{u}} \otimes \underline{\nabla} \rangle + \langle \underset{\sim}{\boldsymbol{\mu}} \rangle : \langle \underset{\sim}{\boldsymbol{\kappa}} \rangle, \tag{36}$$

which defines the effective deformation, curvature, force and couple-stress tensors. The effective medium then is a Cosserat continuum.

3.1.3. Retained approach for non-linear multi-phase materials

The polycrystal is a heterogeneous material with a disordered distribution of phases, each phase being a crystal orientation, and Hill–Mandel approach has proved to be efficient for deriving effective properties in such cases (Sanchez-Palencia and Zaoui, 1985). However, this requires computations on a large representative volume element V containing many grains. Such aggregates have already been computed in classical crystal plasticity (Eberl et al., 1998). But for Cosserat materials, the number of degrees of freedom and internal variables increases drastically in the three-dimensional case so that we will work here on a smaller sample of grains. In the latter case, periodic boundary conditions will induce less pronounced boundary effects than the Dirichlet conditions (24). This is why a mixed approach of Hill–Mandel and periodic ones is retained here, combining the periodic scheme $\mathscr{H}^{\mathrm{II}}$ and unaltered local constitutive equations as in Section 3.1.1 and thus different from Eq. (34). It has been shown numerically in Forest and Sab (1998), at least in the case of linear elasticity, that the approach $\mathscr{H}^{\mathrm{II}}$ works well even if $l_c \sim l$, which will be the case in Sections 4–6.

Accordingly, the following initial boundary value problem $\mathscr{P}$ is considered in a single unit cell V:

$$\begin{aligned} &\underline{\mathbf{u}} = \underset{\sim}{\mathbf{E}} \cdot \underline{\mathbf{x}} + \underline{\mathbf{v}}, \qquad \underline{\boldsymbol{\Phi}} = \underset{\sim}{\mathbf{K}} \cdot \underline{\mathbf{x}} + \underline{\boldsymbol{\psi}}, \\ &\text{constitutive equations,} \\ &\underset{\sim}{\boldsymbol{\sigma}} \cdot \underline{\nabla} = 0, \qquad \underset{\sim}{\boldsymbol{\mu}} \cdot \underline{\nabla} - \underset{\sim}{\epsilon} : \underset{\sim}{\boldsymbol{\sigma}} = 0, \end{aligned} \tag{37}$$

where $\underline{\mathbf{v}}$ (resp. $\underline{\boldsymbol{\psi}}$) takes the same value on opposite sides of the cell. The traction and surface couple vectors of two homologous points on opposite sides of V are the opposite. This problem is solved in a *single* cell V and no attempt is made to extrapolate the solution in a regular solution on the entire body, although it may be possible in particular for symmetric $\underset{\sim}{\mathbf{E}}$ or $\underset{\sim}{\boldsymbol{\Sigma}}$ and vanishing $\underset{\sim}{\mathbf{K}}$.

3.2. Finite element implementation of Cosserat periodic conditions

To solve the boundary value problem $\mathscr{P}$, a specific element has been implemented in the object-oriented finite element code ZéBuLoN (Besson and Foerch, 1997). It represents a generalization of the classical periodic element proposed in Débordes et al. (1985) to the case of periodic Cosserat media. The case of non-periodic Cosserat media has been treated in De Borst (1991, 1993). Two (resp. three) translational and one (resp. three) rotational degrees of freedom $\underline{\mathbf{v}}$ and $\underline{\boldsymbol{\psi}}$ are attributed to each node of the finite element mesh in the two (resp. three)-dimensional case. Furthermore, a set of elements (in practice the whole mesh) shares seven (resp. 18) additional degrees of freedom that are the given tensors $\underset{\sim}{\mathbf{E}}$ and $\underset{\sim}{\mathbf{K}}$. A $7 \times (7+3N)$ (resp. $18 \times (18+6N)$) matrix $[B]$ connects the vector of degrees of freedom $\{\mathrm{dof}\}$ to the generalized deformation vector $\{e\}$:

$$\{e\} = [B]\{\mathrm{dof}\}, \tag{38}$$

where

$$\{e\} = [e_{11}\ e_{22}\ e_{33}\ e_{12}\ e_{21}\ \kappa_{31}\ \kappa_{32}]^{\mathrm{T}}, \tag{39}$$

$$\{\mathrm{dof}\} = [E_{11}\ E_{22}\ E_{33}\ E_{12}\ E_{21}\ K_{31}\ K_{32}\ v_1\ v_2\ \psi_3\ \cdots]^{\mathrm{T}}, \tag{40}$$

$$[B] = \begin{bmatrix} [I_7] & [0] \\ [0] & [b]^{\mathrm{T}} \end{bmatrix} \quad \text{with} \quad [b] = \begin{bmatrix} \frac{\partial}{\partial x} & 0 & 0 & \frac{\partial}{\partial y} & 0 & 0 & 0 \\ 0 & \frac{\partial}{\partial y} & 0 & 0 & \frac{\partial}{\partial x} & 0 & 0 \\ 0 & 0 & 0 & 1 & -1 & l_{\mathrm{n}}\frac{\partial}{\partial x} & l_{\mathrm{n}}\frac{\partial}{\partial y} \end{bmatrix} \tag{41}$$

in the two-dimensional case (plane strain), N being the number of nodes in the element. The 7×7 identity matrix is denoted by $[I_7]$. The normalization length l_{n} has a priori the same order of magnitude as l_{c} and can help in better conditioning of the rigidity matrix.

Elastoviscoplastic constitutive equations as presented in Sections 2.2 and 2.3 enable one to compute the generalized stress vector:

$$\{\sigma\} = [\sigma_{11}\ \sigma_{22}\ \sigma_{33}\ \sigma_{12}\ \sigma_{21}\ \mu_{31}\ \mu_{32}]^{\mathrm{T}}. \tag{42}$$

To deal with single crystals, a three-dimensional formulation has been implemented. The resolution is based on the discretization of the weak formulation of equilibrium:

$$\int_V (\underset{\sim}{\boldsymbol{\sigma}} : \dot{\underset{\sim}{\mathbf{e}}} + \underset{\sim}{\boldsymbol{\mu}} : \dot{\underset{\sim}{\boldsymbol{\kappa}}})\,\mathrm{d}V = \int_V (\underline{\mathbf{f}} \cdot \dot{\underline{\mathbf{u}}} + \underline{\mathbf{c}} \cdot \dot{\underline{\boldsymbol{\Phi}}})\,\mathrm{d}V + \int_{\partial V} (\underline{\mathbf{t}} \cdot \dot{\underline{\mathbf{u}}} + \underline{\mathbf{m}} \cdot \dot{\underline{\boldsymbol{\Phi}}})\,\mathrm{d}S \tag{43}$$

for all virtual fields $\dot{\underline{\mathbf{u}}}$ and $\dot{\underline{\boldsymbol{\Phi}}}$, and where volume forces and micro-couples, and surface tractions and couples may be applied.

The main advantage of introducing additional degrees of freedom associated with the mean deformation $\underset{\sim}{\mathbf{E}}$ and mean curvature $\underset{\sim}{\mathbf{K}}$, is that the associated reactions simply are the mean stresses $\underset{\sim}{\boldsymbol{\Sigma}}$ and $\underset{\sim}{\mathbf{M}}$, so that mean stress-controlled tests can be simulated as well as mean deformation tests. Mixed conditions are therefore also possible.

4. Grain size effects in polycrystal plasticity

4.1. On periodic polycrystalline aggregates

Polycrystalline aggregates containing a large number of grains have been studied in Cailletaud and Quilici (1997) and Eberl et al. (1998), in order to analyse precisely the intragranular stress-deformation state inside a representative volume element V within the framework of classical crystal plasticity. For this purpose, homogeneous Dirichlet boundary conditions have been used. If V contains a large enough number of grains, the overall response is found to coincide with the prediction of a self-consistent polycrystal model (Quilici et al., 1998). Parallel computing is necessary to deal with representative samples of polycrystalline material. The so-called multi-phase element technique is used, where each integration point of the FE mesh is given the particular properties of the grain it belongs to. More precisely the single crystal model described in Section 2.2 is used at each integration point with the crystallographic orientation of the corresponding grain in the polycrystalline material. The definition of the micro-structure is based upon a synthetic polycrystalline aggregate generated by disposing nucleation points in a cube of unit length and applying an isotropic growth law to obtain an equiaxed micro-structure (Voronoï polyhedra) (Decker and Jeulin, 1998). The distribution of nuclei follows a Poisson distribution. Decker and Jeulin (1998) have also added to the previous polycrystal generation procedure the constraint that the distribution be periodic. It means that grains crossing the boundary of the cube are in correspondence on opposite faces (Fig. 2).

In this section, we investigate aggregates of Cosserat grains with a rather small number of grains so that we can resort to sequential calculations. Periodicity conditions are prescribed on both the micro-structure geometry and on the mechanical quantities $\underline{\mathbf{v}}$ and $\underline{\underline{\psi}}$ (boundary value problem $\mathscr{P}$). Samples of 10 grains are considered using a $10 \times 10 \times 10$ linear element mesh. This leads to a number of about 800 Gauss points per grain that is sufficient for a realistic approximation of the 3D stress–strain gradients inside each grain. This is an upper limit for sequential computation on a workstation using the Cosserat model.

Instead of constructing the effective response of a polycrystal using a large volume V containing many grains, it is possible to study several samples including a smaller number of grains with periodicity

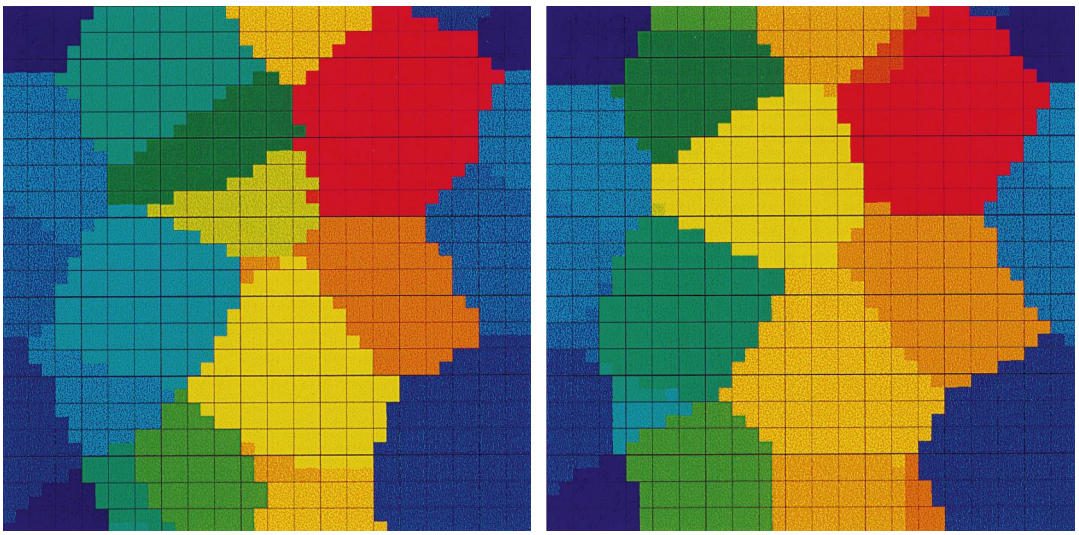

Fig. 2. Two successive slices of a three-dimensional polycrystalline aggregate and the associated mesh using the multi-phase element technique; note the periodicity conditions.

conditions. A mean response over a large enough number of realizations can be computed and regarded as an estimation of the ensemble average of the studied mechanical quantity. According to the ergodic hypothesis, the two approaches should coincide. The quality of the estimation depends on the number of realizations and on the number of heterogeneities considered in each sample. This approach is similar to the treatment of macro-heterogeneous solids proposed in (Huet, 1990). A sample of 10 grains may then provide only a lower bound for the overall response. Alternatively, each periodic aggregate of 10 grains can be regarded as a very special polycrystalline material for which we obtain the exact effective response.

In this work, we are interested in the response of polycrystals to classical loading conditions, such as prescribed symmetric mean deformation or stress. In all calculations presented, the mean curvature $\underset{\sim}{\mathbf{K}}$ is set to zero. In the case of a tensile test, the component E_{33} is prescribed, $\sum_{33}$ is computed and the remaining components of $\underset{\sim}{\boldsymbol{\Sigma}}$ vanish. It is often advocated that the additional boundary conditions that arise in structural calculations involving generalized continua, are difficult to set. In the case of single crystals, direct control of lattice rotation is impractical. In contrast, periodic conditions on $\underline{\boldsymbol{\psi}}$ in problem $\mathscr{P}$ are natural.

4.2. Finite element analysis

The following series of systematic calculations have been carried out. A cube is considered that contains 10 grains with approximately the same size and shape. One special orientation is attributed to each grain according to a random process. Two samples A and B have been generated with two different geometry and orientation distribution. The orientations A and B are given on Fig. 3. The material behaviour of each grain is described by the set of constitutive equations of Cosserat elastoviscoplasticity given in Sections 2.2 and 2.3. Table 1 gives the values of the material parameters for the simulation. They have been retained for illustration only, but they correspond to the behaviour of the polycrystalline alloy IN600. F.c.c. crystals are considered and the 12 octahedral slip systems $\{1\,1\,1\}\ \langle 0\,1\,1\rangle$ are taken into account. The parameter H' entering the hardening rule (21) has been arbitrarily set to 10 000 MPa and l_p to 0.1 mm. The edge length d of the cube is varied in this study. For a given polycrystalline sample (A or B), the grain geometry, the number of grains, the initial orientation of the grains and the material parameters are kept constant, whereas the absolute size d of the aggregate and therefore the grain size varies from one simulation to the

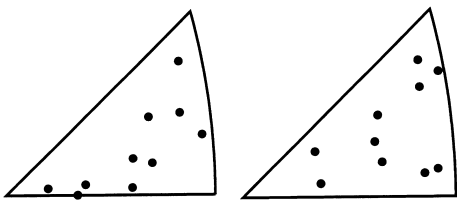

Fig. 3. Stereographic projections of the tensile axis in the 10 grains of samples A (left) and B (right).

Table 1
Material parameters used for the simulation of grain size effects in polycrystals (the classical parameters and the specific Cosserat parameters have been separated)

E (MPa)	ν	r_0 (MPa)	q (MPa)	b	h_{ij}	k (MPa$^{1/n}$)	n	μ_c (MPa)	β (MPa m^2)	r_{0c} (MPa)	H' (MPa)	l_p (mm)	k_c (MPa$^{1/n_c}$)	n_c
196 000	0.3	111	35	7	1	10	20	500 000	0.0001	10^{-6}	10 000	0.1	0.1	1

other. In particular, parameter H' is regarded as a material parameter and will not be changed when changing the size of the cube: its value determines the minimum grain size for which Cosserat effects will arise. It should be fitted once for all on experimental responses including several grain sizes.

A large spectrum of grain sizes has been explored ranging from $d = 1\,\mu m$ to $d = 1\,mm$. The influence of grain size on the overall mechanical response of the aggregate A and B in pure tension is first investigated. Results are reported in Fig. 4(a) and (b) for samples A and B. For d greater than 1 mm, the response is not affected and corresponds to that of a classical Cauchy material: no Cosserat effect arises. For smaller grain sizes, the material can harden substantially more than for the classical case. For very fine grains, a very strong additional hardening is obtained. This additional hardening is attributed to the coupling term driven by parameter H' and can be understood as follows: The threshold of micro-plasticity is the same for all grain sizes, so that the local fields are comparable at the very beginning of plastic flow. In particular, lattice rotations are firstly very similar but lattice curvature strongly differs due to the different value of distances associated with absolute coordinate $\underline{\mathbf{x}}$. The greater the plastic curvature $\underset{\sim}{\boldsymbol{\kappa}}^{p}$, the smaller is the grain. Plastic

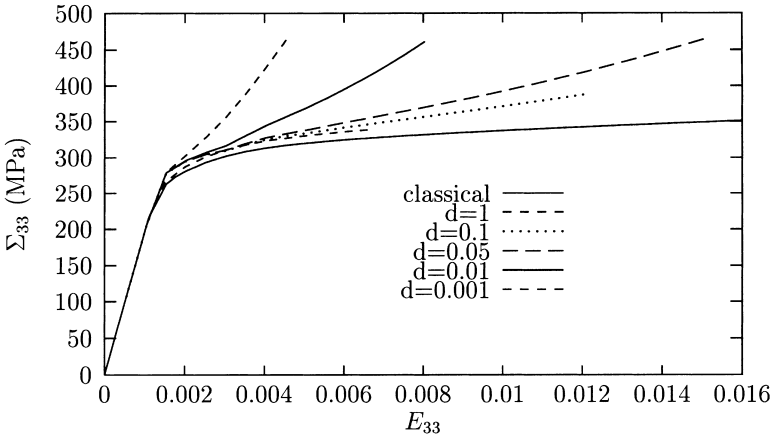

(a)

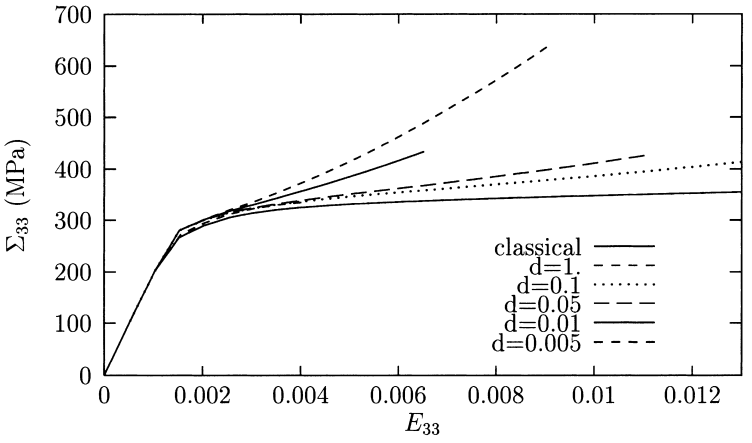

(b)

Fig. 4. Tensile tests on a periodic polycrystalline aggregate for different grain sizes: (a) sample A, (b) sample B.

curvature is related to the ratio θ^s/l_p via Eq. (18). Since l_p is kept constant, the internal variable θ^s is bigger for small grains and hence the contribution $H'\theta^s$ is stronger and may become predominant. The key point in the analysis is the ratio of the relative contributions of the term $q\sum_{r=1}^{n} h^{sr}(1-\exp(-bv^r))$ and the term $H'|\theta^s|$ in the hardening rule (21). When d is much greater than l_p, plastic curvature and therefore the variable θ^s are very small so that the additional term provides a negligible contribution. In contrast, for $d \sim l_p$ and $d < l_p$, the contribution of geometrically necessary dislocations becomes predominant, as explained above. Effects due to local plastic curvatures seem to affect the hardening behaviour of the material only and not the apparent initial yield strength. However, for a high parameter H', the overall response mimics elasticity. The use of a non-linear coupling term would then allow the simulation of a subsequent non-linear response. It means that the proposed framework can account for a dependence of both the hardening behaviour and the initial apparent yield strength of polycrystalline aggregates on grain size. The simulations on sample B confirm the previous analysis and the effects observed on the overall response have the same order of magnitude. The effect of grain size on the overall behaviour may also depend on the loading conditions. In Fig. 5, we consider a test for which all components of the mean deformation tensor are prescribed and are proportional to

$$E_{33} = 1, \quad E_{11} = E_{22} = -0.5,$$

the remaining components being set to zero. The elastic response of the material here is compressible, so that these loading conditions result in higher stress values and triaxiality. The obtained results are similar to that in pure tension.

To quantify the hardening effect of the grain size, we plot $\log(\Sigma_{33} - \Sigma_0)$ versus $\log(d)$ in Fig. 6 for the three investigated cases. For a given value, E_{33}, Σ_0 denotes the stress response of the size-independent classical material. Note that the response of the classical medium is slightly lower than the response of the Cosserat medium with large grains, this is due to the influence of the coarse mesh. The curves obtained over a large range of grain sizes can almost be described by a straight line of slope between -0.7 and -0.4. This scaling turns out to be compatible with a Hall–Petch type relation. It must be noted that this non-linear relationship between additional hardening and grain size is obtained using a linear Cosserat coupling term. The non-linearity stems from plastic curvature distribution inside the grains (Fig. 7(d)). Fig. 7(a) shows a slice of sample A where six grains can be observed. The plastic deformation and lattice rotation patterns of Fig. 7(b) and (c) cannot be simply related to the grain distribution. In contrast, the contour of plastic curvature suggests that plastic curvature does not develop in the core of the grain but at the grain boundaries (Fig. 7(d)). This is compatible with the fact that lattice rotations are quite homogeneous in the core of the grain (Fig. 7(c)) and become heterogeneous near the grain boundaries. However, computations

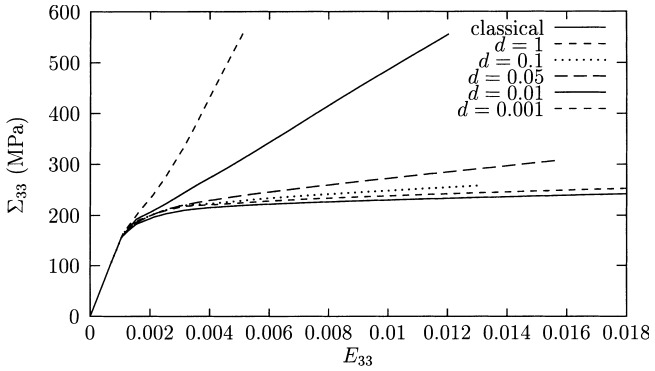

Fig. 5. Deformation controlled tests on a periodic polycrystalline aggregate for different grain sizes (sample A).

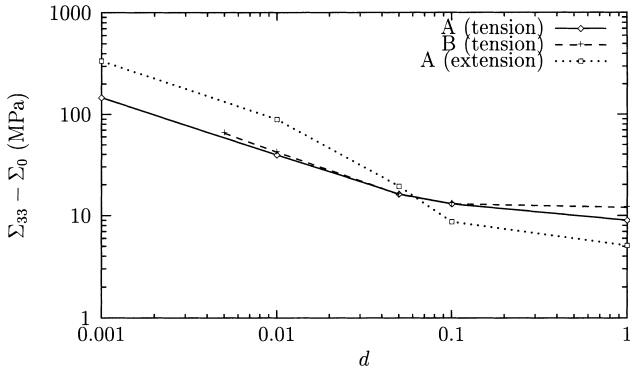

Fig. 6. Relationship between stress and grain size at a given prescribed $E_{33} = 0.0045$ strain and for pure tensile test and tests with a controlled mean deformation (called here "extension").

with a finer mesh must be carried out to confirm this feature of grain plasticity. The effect of grain size on the local fields is shown in Fig. 8. The three-dimensional plastic deformation state of aggregate A is given for a mean value $E_{33} = 0.0045$ for two different grain sizes. At the early stage of deformation, the shape of the plastically activated grains can be recognized. The maximum plastic deformation reached locally for $d = 0.005$ mm is almost twice less than for $d = 0.1$ mm. This results in a very different partition of total deformation into elastic and plastic parts, in both cases.

5. Towards a field theory of precipitate hardening

Homogenization methods are of no help to predict the effective elasticity constants of an alloy made of elements A and B, from the knowledge of the elastic properties of A and B alone and of the composition of the alloy. This is the realm of physical metallurgy and the adequate numerical tool rather is atomic simulation. In the same way, the description of precipitate hardening does not fall a priori into the field of continuum mechanics. However, when the material contains large enough precipitates or inclusions, the hardening effect may involve a large enough amount of dislocations for non-local continuum plasticity to become applicable. A two-dimensional example of the transition from discrete dislocation dynamics to continuum plasticity has been provided in Cleveringa et al. (1998). The size of γ' precipitates in nickel-based single crystal superalloys lies in a range for which discrete methods require a tremendous computational effort and generalized continuum crystal plasticity may start to be applicable.

5.1. On the modelling of two-phase single crystal nickel-based superalloys

Nickel-based single crystal superalloys for high temperature applications contain a large volume fraction of coherent γ' precipitates in a matrix of disordered phase γ. Espié (1996) has been able to grow single crystals made of the phase γ alone and could study their mechanical properties. The γ phase turns out to be very soft at a high temperature, as shown in Fig. 9(a). The high volume fraction of γ' precipitates confers a very strong reinforcement to the alloy until they are sheared by dislocations. Several micro-mechanical models have been proposed to reconstruct the behaviour of the heterogeneous material starting from the knowledge of the mechanical response of each individual phase. A self-consistent scheme has been proposed in Forest and Pilvin (1996), whereas periodic homogenization has been resorted to in Nouailhas and

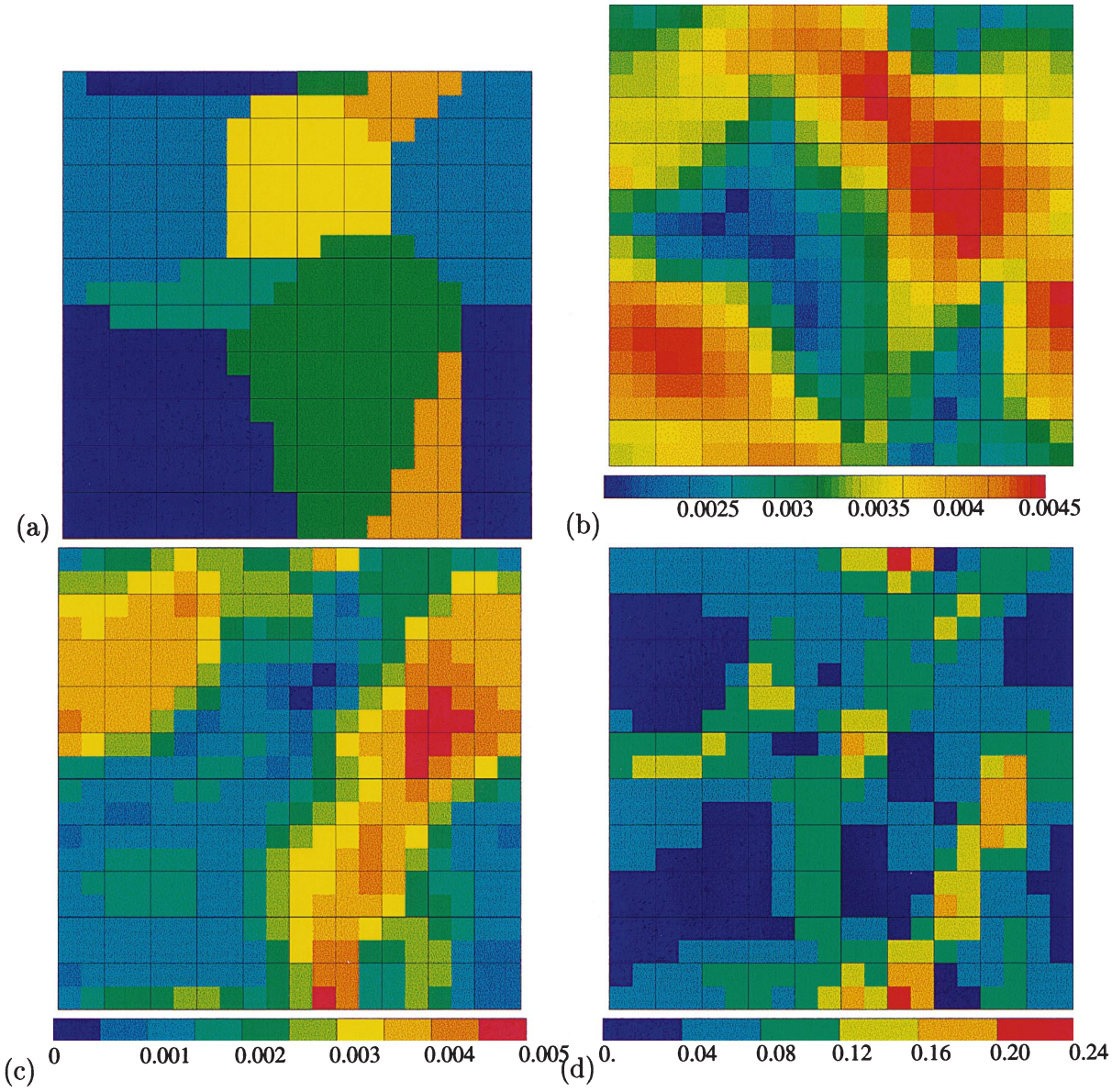

Fig. 7. Section of a periodic polycrystalline aggregate: (a) grain distribution, (b) equivalent plastic strain field, (c) norm of the lattice rotation vector field and (d) equivalent plastic curvature.

Cailletaud (1995, 1996). Both approaches fail to predict the yield stress of the material (see Fig. 9(a)). The reason simply is that the dislocation behaviour in the narrow channels of the γ matrix dramatically differs from the plastic behaviour of the bulk γ phase. This is of course a well-known metallurgical fact and the increase of the effective yield stress can be correctly estimated by a Orowan-type contribution proportional to the inverse of the matrix channel width. Accordingly, Espié (1996) modifies the local hardening rule of phase γ as follows:

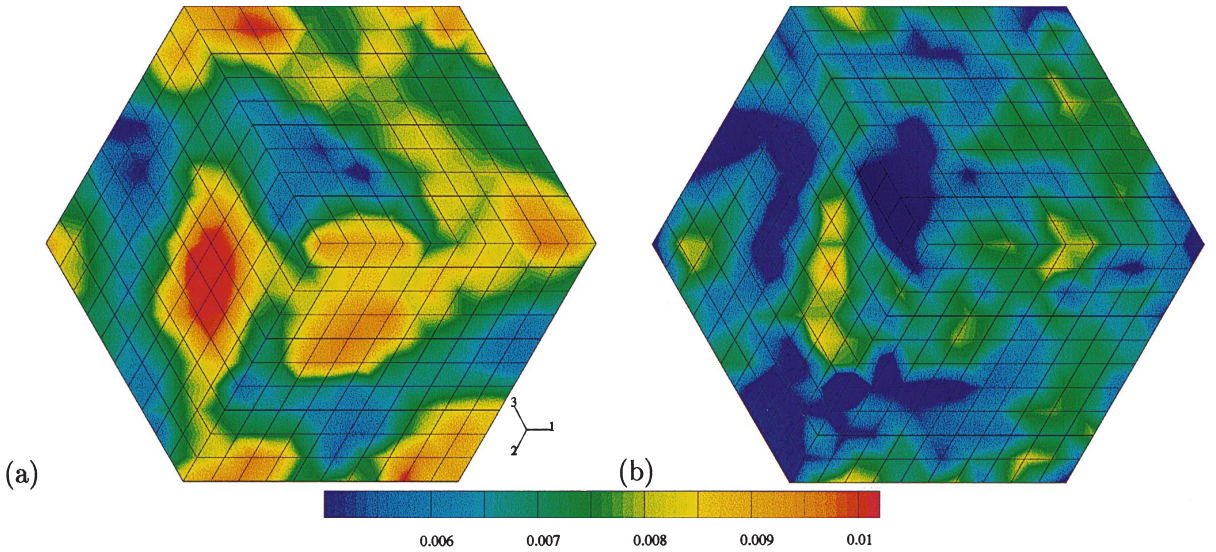

Fig. 8. Deformation controlled test on a periodic polycrystalline aggregate for different grain sizes (sample *A*): Cumulative plastic deformation for (a) $d = 0.1$ mm, (b) $d = 0.005$ mm.

$$r^s = r_0 + \alpha\frac{C_{44}b}{d} + q\sum_r h^{sr}(1 - \mathrm{e}^{-bv^r}), \tag{44}$$

where b is the norm of Burgers vector, C_{44}, the shear modulus of cubic elasticity and α, a material parameter to be fitted. However, the Orowan contribution mainly has a macroscopic meaning and, in principle, should not be applied indifferently at each position in the γ-channels in a unit cell calculation. In contrast, here we propose to use Cosserat plasticity and to investigate whether the plastic curvature in the γ-channels is sufficient to account for the observed apparent higher strength.

5.2. Tensile behaviour

The tensile behaviour of γ/γ' single crystal superalloy AM1 in direction [0 0 1] is first investigated using periodic homogenization. The precipitates have a cuboidal shape and only one-eighth of the entire unit cell is necessary (Fig. 9(b)). The dimensions of the cell correspond to the actual mean precipitate sizes in AM1: 0.56 μm-long precipitate edges and 0.08 μm-wide channels. The actual rounded shape of the corners of the cubes has been taken into account, although a rather coarse mesh is used that permits sequential three-dimensional calculations with the Cosserat model. The material parameters used for each phase are listed in Table 2. The parameters of γ are exactly the same as for the bulk material and have been deduced from tensile tests (Espié, 1996). The coupling term H' of Cosserat plasticity does not influence the homogeneous tensile response but will play a major role when γ is inhomogeneously strained in the channels. At the considered temperature of 950°C, the mechanical behaviour of the material is highly viscoplastic. Octahedral slip systems only have been retained, although cubic slip plays a major role in particular for tensile tests in direction $\langle 1\,1\,1\rangle$ (Nouailhas and Cailletaud, 1995; Espié et al., 1995). Climb processes are significantly active at high temperature, and they are not taken into account from the crystallographic point of view here but via the viscosity parameters. For simplicity, the same elastic properties have been attributed to each phase and the misfit between the two coherent phases has been neglected. The γ'-phase is regarded

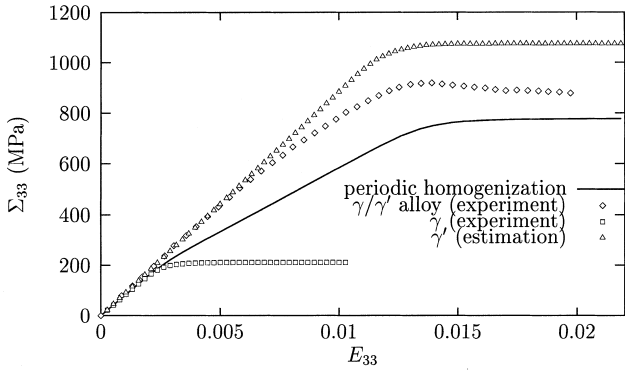

(a)

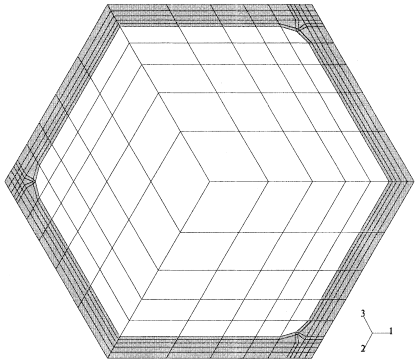

(b)

Fig. 9. (a) Tensile tests on AM1 single crystal superalloy (950°C, $\dot{E}_{33} = 10^{-3}$ s^{-1}, after Espié (1996)): γ-phase and γ′-phase bulk materials, γ/γ' superalloy and prediction of the effective response using periodic homogenization; (b) mesh of the unit cell used for the periodic homogenization analysis.

Table 2
Material parameters for the γ and γ′ phases used in the simulation of the behaviour of Ni-based single crystal superalloys

	C_{11} (MPa)	C_{12} (MPa)	C_{44} (MPa)	r_0 (MPa)	q (MPa)	b	h_{ij}	k (MPa$^{1/n}$)	n	μ_c (MPa)	β (MPa m^2)	r_{0c} (MPa)	H' (MPa)	l_p (mm)	k_c (MPa$^{1/n_c}$)	n_c
γ	137 000	78 000	111 000	36	5.2	5800	δ_{ij}	190	5	1 000 000	0.00001	10^{-6}	varying	0.0001	0.01	1
γ′	137 000	78 000	111 000	350	17	5800	δ_{ij}	300	5	1 000 000	0.00001	10^{-6}	0	0.0001	0.01	1

as shearable only for a high critical resolved shear stress. This is assumed to be the reason for the softening observed on the experimental curve of Fig. 9(a). Whereas the parameter H' has been kept constant in the analysis of different grain sizes in Section 4, here we study the influence of H' on the additional hardening obtained for a fixed size of the micro-structure.

Fig. 10 shows that for sufficiently high values of H', there is enough plastic curvature in the phase γ to make the overall response look like elasticity until high stress levels, although the threshold of micro-plasticity in γ remains unchanged. Due to the choice of a linear coupling term, the apparent elastic response stopped only with the yielding of the γ′ phase. The value of H' found to account for the experimental data seems to be very high and perhaps unrealistic. It suggests that the lattice curvature in the matrix channel is an important point to explain the reinforcement in the γ/γ' but may not be the only one. At the beginning

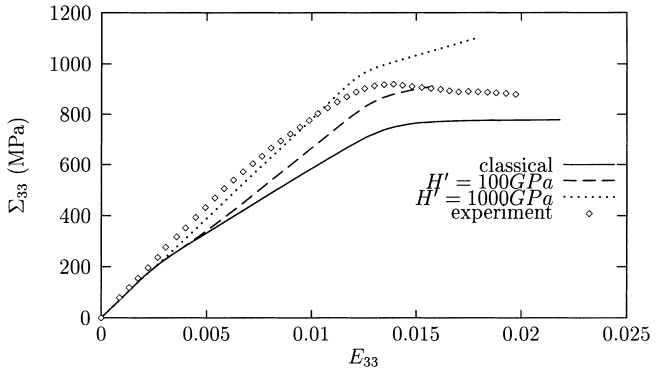

Fig. 10. Tensile tests on the γ/γ' unit cell for different coupling moduli H'.

of plastic flow in the matrix, the plastic curvature essentially develops at the intersection of γ channels, at γ' corners. The additional hardening associated with it leads to subsequent stress redistributions. Accordingly, the zone where lattice rotation takes place, spreads over a larger region than in the classical case, as shown in Fig. 11.

5.3. Shear behaviour

Once material parameters have been identified, their relevance can be checked for different loading conditions. Torsion tests on single crystals are complex and careful measurements must be interpreted using finite element computations since the torsion of single crystal tubes leads to a non-homogeneous deformation along the circumference (Nouailhas and Cailletaud, 1995). Considering the simple shear test on a γ/γ' unit cell and using classical crystal plasticity with parameters identified from tensile tests, Nouailhas

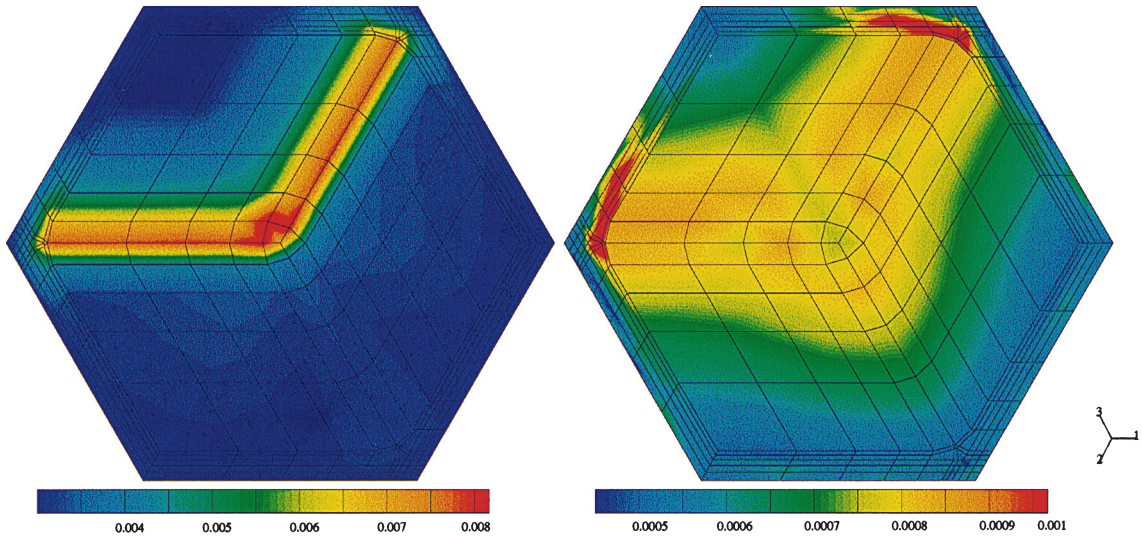

Fig. 11. Norm of the lattice rotation vector in the γ-phase for $E_{33} = 0.008$: Classical case (left) and Cosserat crystal (right, with $H' = 1000$ MPa).

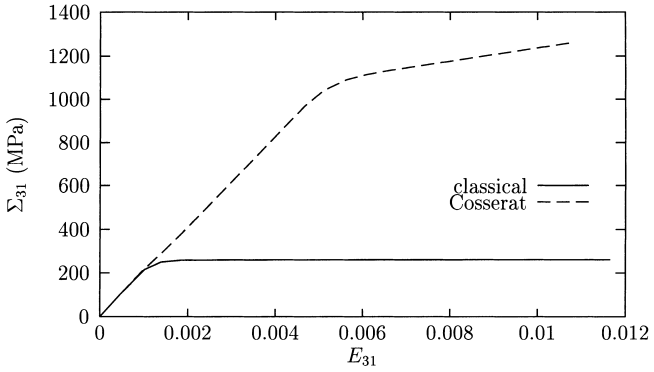

Fig. 12. Simple shear tests on the γ/γ' unit cell for the classical case and for Cosserat with $H' = 1000$ GPa.

(1997) predicts a response which is too soft when compared to experiment. This is due to the fact that, using periodicity conditions, the γ-phase is strongly sheared, whereas the precipitate remains almost undeformed. It must be noted that, in the self-consistent scheme used in (Forest and Pilvin, 1996), the γ/γ' composite assembly is embedded in the homogeneous equivalent medium and the pure shear conditions are prescribed at infinity which leads to a more complex deformation state in the composite inclusions and to a harder response. However, we stick here to the periodic assumption and use the same Cosserat model for γ and γ' as for the tensile test. The shearing plane is a (0 1 0) plane and the shearing direction is [1 0 0]. A much stronger response of the material is obtained than with the classical model (Fig. 12). Again, the use of linear coupling becomes unrealistic and the γ' precipitate is finally plastically sheared. Note that, for such an orientation, a cubic slip would be significantly activated and its introduction is necessary for quantitative comparison with experiment.

6. Conclusions

The mechanics of generalized continua has been shown to be an appropriate tool to account for size effects in polycrystal and multi-phase materials. Cosserat single crystal plasticity gives rise to Hall–Petch-type grain size effects in periodic polycrystalline aggregates. Various possible homogenization approaches have led us to formulate an initial boundary value problem of Cosserat elastoviscoplasticity with periodicity conditions for both the micro-structure and the mechanical fields. Rather small polycrystalline samples have been considered in this work, and the next step will be to carry out large scale parallel computations on multi-processor computers as has been done in the classical case (Eberl et al., 1998). In the presented simulations, the local fields can be significantly different from those observed in classical crystal plasticity, due to stress redistributions following additional hardening in the domain of large plastic lattice curvature. This has been shown also in the case of two-phase materials. Grain boundaries are privileged sites for the development of a strong lattice curvature. However, a disadvantage of the multi-phase element technique is that interfaces become serrated surfaces and are not well described. This method can exaggerate some observed boundary effects. A quantitative comparison between this method and the use of properly meshed grain boundaries is reported in Cailletaud and Quilici (1997). The following question arises: how far is the response of a rather small periodic aggregate of crystals from the actual response of the polycrystal? The work of Drugan and Willis (1996) in the case of composite materials requires a rather small amount of heterogeneities to estimate the overall response of the material, provided that ensemble averaging is used. This means that several computations must be carried out for various samples (such as A and B in Section

4), followed by an averaging procedure. Statistical methods should be applied to quantify the minimal number of grains in the cell and of realizations that are necessary to obtain a given precision on the overall response of the polycrystal. The alternative method consists in computing a representative volume element containing as many grains as possible, which remains a challenging issue for parallel computing. Similarly, parallel computing should be resorted to for an improved treatment of γ/γ' single crystal superalloys, for which a rather crude mesh has been used in Section 5. It appears in both analyses of grain size effect and precipitate hardening that the linear form (21) is not sufficient for a quantitative agreement with experimental data. A non-linear form displaying a saturation would be more realistic and will require an additional material parameter. The mechanics of generalized continua is a tool that can be resorted to when the size of the considered heterogeneities lies still beyond the computational capabilities of discrete simulations and is such that classical constitutive equations fail. This has been illustrated in the case of single crystal superalloys for which the additional hardening due to the constrained deformation in the matrix channels has been captured. The relevance of the prediction has been tested in simple shear and should be applied to another precipitate size for the same volume fraction.

References

Besson, J., Foerch, R., 1997. Large scale object-oriented finite element code design. Computer Methods in Applied Mechanics and Engineering 142, 165–187.

Boutin, C., 1996. Microstructural effects in elastic composites. International Journal of Solids and Structures 33, 1023–1051.

Cailletaud, G., Quilici, S., 1997. Calculs parallèles d'agrégats multicristallins. In: DRET Report Fundamental Research Program, Ecole des Mines de Paris.

Cleveringa, H., Van der Giessen, E., Needleman, A., 1998. Discrete dislocation simulations and size dependent hardening in single slip. Journal de Physique IV France 8, Pr4-83–92.

Dai, H., Parks, D.M., 1997. Geometrically-necessary dislocation density and scale-dependent crystal plasticity. In: Khan, A.S. (Ed.), Proceedings of Plasticity '97. Neat Press, Fulton, Maryland, pp. 17–18.

Débordes, O., Licht, C., Marigo, J.J., Mialon, P., Michel, J.C., Suquet, P., 1985. Calcul des charges limites de structures fortement hétérogènes. In: Grellier, J.P. (Ed.), Tendances actuelles en calcul de structures. Pluralis, France, pp. 56–70.

Decker, L., Jeulin, D., 1998. Simulations 3D de matériaux aléatoires. Mémoires Scientifiques de la Revue de Métallurgie, in press.

De Borst, R., 1991. Simulation of strain localization: a reappraisal of the Cosserat continuum. Engineering Computations 8, 317–332.

De Borst, R., 1993. A generalization of J_2-flow theory for polar continua. Computer Methods in Applied Mechanics and Engineering 103, 347–362.

De Felice, G., Rizzi, N., 1997. Homogenization for materials with microstructure. In: Kwon, Y.W., Davies, D., Chung, H.H., Librescu, L. (Eds.), Recent Advances in Solids/Structures and Application of Metallic Materials, PVP-vol. 369, ASME, New York.

Dendievel, R., Forest, S., Canova, G., 1998. An estimation of overall properties of heterogeneous Cosserat materials. Journal de Physique IV France 8, Pr8-111–118.

Drugan, W.J., Willis, J.R., 1996. A micromechanics-based nonlocal constitutive equation and estimates of representative element size for elastic composites. Journal of the Mechanics and Physics of Solids 44, 497–524.

Eberl, F., Feyel, F., Quilici, S., Cailletaud, G., 1998. Approaches numériques de la plasticité cristalline. Journal de Physique IV France 8, Pr4-15-25.

Eringen, A.C., 1976. Polar and nonlocal field theories. In: Continuum Physics, vol. 4. Academic Press, London.

Espié, L., Hanriot, F., Cailletaud, G., Rémy, L., 1995. Application of crystallographic viscoplastic constitutive equations to nickel-base superalloys. In: Bakker, A. (Ed.), Seventh International Conference on Mechanical Behavior of Materials. ESIS, The Hague, Netherlands.

Espié, L., 1996. Etude expérimentale et modélisation numérique du comportement mécanique de monocristaux de superalliages. Doctoral Thesis, Ecole des Mines de Paris.

Fivel, M., Canova, G., 1998. Simulations 3D de dislocations en conditions aux limites complexes. Journal de Physique IV France 8, Pr4-249–258.

Fleck, N.A., Hutchinson, J.W., 1997. Strain gradient plasticity. Advances in Applied Mechanics 33, 295–361.

Forest, S., Pilvin, P., 1996. Modelling the cyclic behaviour of two-phase single crystal nickle-base superalloys. In: Pineau, A., Zaoui, A. (Eds.), IUTAM Symposium on Micromechanics of Plasticity and Damage of Multiphase Materials. Kluwer Academic Publishers, Dordrecht, Netherlands, pp. 51–58.

Forest, S., Cailletaud, G., Sievert, R., 1997. A Cosserat theory for elastoviscoplastic single crystals at finite deformation. Archives of Mechanics 49, 705–736.

Forest, S., 1998. Modeling slip, kink and shear banding in classical and generalized single crystal plasticity. Acta Materialia 46, 3265–3281.

Forest, S., Sab, K., 1998. Overall modelling of periodic heterogeneous Cosserat media. In: Inan, E., Markov, K.Z. (Eds.), Ninth International Symposium on Continuum Models and Discrete Systems. World Scientific, Singapore, pp. 445–453.

Germain, P., 1973. La méthode des puissances virtuelles en mécanique des milieux continus premiere partie: théorie du second gradient. Journal de Mécanique 12, 235–274.

Huet, C., 1990. Application of variational concepts to size effects in elastic heterogeneous bodies. Journal of the Mechanics and Physics of Solids 38, 813–841.

Jaoul, B., 1965. Etude de la plasticité et application aux métaux. Dunod, Paris.

Koiter, W.T., 1960. Progress in Solid Mechanics, vol. 1. North-Holland, Amsterdam, pp. 165–221.

Koiter, W.T., 1963. Couple-stresses in the theory of elasticity I and II. Proc. K. Ned. Akad. Wet. B 67, 17–44.

Kröner, E., 1958. Kontinuumstheorie der Versetzungen und Eigenspannungen. Ergebnisse der angewanten Mathematik, vol. 5, Springer, Berlin.

Kröner, E., 1963. On the physical reality of torque stresses in continuum mechanics. International Journal of Engineering Science 1, 261–278.

Kröner, E., 1969. Initial studies of a plasticity theory based upon statistical mechanics. In: Kanninen, M.F., Adler, W.F., Rosenfield, A.R., Jaffee, R.I., (Eds.), Inelastic Behaviour of Solids. McGraw-Hill, New York, pp. 137–147.

Mandel, J., 1965. Généralisation de la théorie de plasticité de W.T. Koiter. International Journal of Solids and Structures 1, 273–295.

Mandel, J., 1971. Plasticité classique et viscoplasticité. CISM, Udine, Springer, Berlin.

Mandel, J., 1973. Equations constitutives et directeurs dans les milieux plastiques et viscoplastiques. International Journal of Solids and Structures 9, 725–740.

Nouailhas, D., Cailletaud, G., 1995. Tension–torsion behaviour of single crystal superalloys: Experiment and finite element analysis. International Journal of Plasticity 11, 451–470.

Nouailhas, D., Cailletaud, G., 1996. Finite element analysis of the mechanical behaviour of two-phase single crystal superalloys. Scripta Materialia 34, 565–571.

Nouailhas, D., 1997. Finite element modelling of single crystal superalloy behaviour. In: Khan, A.S. (Ed.), Proceedings of Plasticity '97, Neat Press, Fulton, Maryland, pp. 17–18.

Nye, J.F., 1953. Some geometrical relations in dislocated crystals. Acta Metallurgica 1, 153–162.

Quilici, S., Forest, S., Cailletaud, G., 1998. On size effects in torsion of multi- and polycrystalline specimens. Journal de Physique IV France 8, Pr8-325–332.

Sanchez-Palencia, E., 1974. Comportement local et macroscopique d'un type de milieux physiques hétérogènes. International Journal of Engineering Science 12, 331–351.

Sanchez-Palencia, E., Zaoui, A., 1985. Homogenization techniques for composite media. Lecture notes in physics 272, Springer, Berlin.

Shu, J.Y., Fleck, N.A., King, W.E., 1996. Bicrystals with strain gradient effects. In: Proceedings of MRS Fall Meeting. Symposium W.

Sievert, R., Forest, S., Trostel, R., 1998. Finite deformation Cosserat-type modelling of dissipative solids and its application to crystal plasticity. Journal de Physique IV 8, Pr8-357–364.

Smyshlyaev, V.P., Fleck, N.A., 1996. The role of strain gradients in the grain size effect for polycrystals. Journal of the Mechanics and Physics of Solids 44, 465–495.

Weng, G.J., 1983. A micromechanical theory of grain-size dependence in metal plasticity. Journal of the Mechanics and Physics of Solids 31, 193–203.